J. CHEM. SOC. FARADAY TRANS., 1994, 90(12), 1569–1574

Some Thoughts on Reaction-path Following

H. Bernhard Schlegel
Department of Chemistry, Wayne State University, Detroit, MI 48202, USA

Errors in reaction-path following have been examined with the aid of a simple model surface and a local correction scheme has been proposed. Two new fourth-order explicit methods for reaction-path following have been developed, and two potential-energy surfaces with analytical reaction paths have been constructed. Some aspects of reaction-path bifurcation are also discussed.

In exploring a potential-energy surface for a reaction, normally the first step is to optimize the geometry of the relevant stationary points, *i.e.* the reactants, transition structure and products.[1] To confirm a reaction mechanism, it may be necessary to prove that the particular transition structure found in the optimization connects the desired reactants and products. This can be done by following the path of steepest descent downhill from the transition structure toward the reactants and toward the products. Following the reaction path can also show whether the mechanism involves any intermediates between reactants and products. Although the path of steepest descent depends on the coordinate system, a change in the coordinate system does not change the nature of the stationary points and does not alter the fact that the energy decreases monotonically along the reaction path from the transition structure toward reactants or products. Thus any coordinate system can be used to explore the mechanism of a reaction. One system, mass-weighted cartesian coordinates, has special significance for reaction dynamics, and the path of steepest descent in this coordinate system is called the intrinsic reaction coordinate (IRC).[2]

The next step in characterizing a reaction in a theoretical study of a potential-energy surface is to calculate the rate of the reaction. At the simplest level, one can use conventional transition-state theory (TST), which depends on the geometry and vibrational modes of the transition structure.[3] If the barrier is low or broad, the dynamic bottleneck may not be at the transition structure, and one needs to use variational transition-state theory (VTST).[4] This requires the reaction path or IRC near the transition state and the vibrational frequencies perpendicular to the path. Tunnelling corrections may also be important and can be estimated from the IRC and the shape of the potential-energy surface near the transition state.

Following reaction paths is, therefore, central to any treatment of reactions on potential-energy surfaces that goes beyond locating transition structures. Methods for computing reaction paths have been reviewed recently.[5,6] Despite their conceptual simplicity, reaction paths are remarkably difficult to follow efficiently and accurately. Many small steps may be needed to follow the path closely, and this can be quite costly if the potential-energy surface is obtained by high-level *ab initio* electronic structure calculations. The reason for these difficulties is that the defining equations for reaction paths belong to a class of stiff differential equations. With this short paper we hope to stimulate discussion by offering two new fourth-order path-following methods, some new test surfaces and a few thoughts on bifurcation of reaction paths.

Definitions

A potential-energy surface $E(x)$ can be expanded as a Taylor series about x_0

$$E(x) = E_0 + g_0^t(x - x_0) + \tfrac{1}{2}(x - x_0)^t H_0(x - x_0) + \cdots \quad (1)$$

where E_0, g_0 and H_0 are the energy, gradient and Hessian at x_0. The reaction path on this surface can also be expanded as a Taylor series

$$x(s) = x(0) + v^0(0)s + \tfrac{1}{2}v^1(0)s^2 + \cdots \quad (2)$$

where s is the arc length along the path, v^0 is the tangent vector, and v^1 is the curvature. The tangent vector for the path of steepest descent is

$$v^0(s) = \frac{dx(s)}{ds} = \frac{-g(x)}{|g(x)|} \quad (3)$$

The curvature can be computed for the Hessian:

$$v^1(s) = -[Hv^0 - (v^{0t}Hv^0)v^0]/|g(x)|; \quad \kappa = |v^1| \quad (4)$$

At the transition structure, the gradient is zero and the tangent is given by the eigenvector of the Hessian corresponding to the negative eigenvalue, and the curvature is given by

$$v^1(s) = -[H - 2(v^{0t}Hv^0)I]^{-1}[F^1v^0 - (v^{0t}F^1v^0)v^0] \quad (5)$$

where $F^1_{ij} = \sum_k F_{ijk}v^0_k$ and F_{ijk} are the third derivatives.

A number of quantities are needed for treatments of reaction rates that go beyond conventional transition-state theory. The vibrational frequencies perpendicular to the reaction path can be obtained by diagonalizing the projected Hessian:

$$H_{proj} = PHP; \quad P = I - v^0v^{0t} \quad (6)$$

The coupling terms between motion along the path and vibrational modes perpendicular to the path are given by:

$$B_{i,s} = \frac{dL_i^t}{ds}v^0 = L_i^t\frac{dv^0}{ds} = L_i^tv^1 \quad (7)$$

where L are the eigenvectors of the projected Hessian. Formulae for other terms appearing in the VTST and reaction-path Hamiltonian treatments of reaction rates can be found in the literature.[7,8]

Bifurcation

Bifurcation is a novel aspect of reaction paths and has been discussed extensively by Ruedenberg[9] and others. A potential-energy surface in which one valley divides into two has a valley-ridge inflection point (VRI). On one side of the VRI, all second derivatives perpendicular to the reaction path are positive, indicating a valley; on the other side, one perpendicular mode has a negative eigenvalue, indicating a ridge. Thus, the VRI is characterized by a zero eigenvalue for the second derivatives perpendicular to the path. Baker and Gill[10] have published an algorithm for locating VRIs on

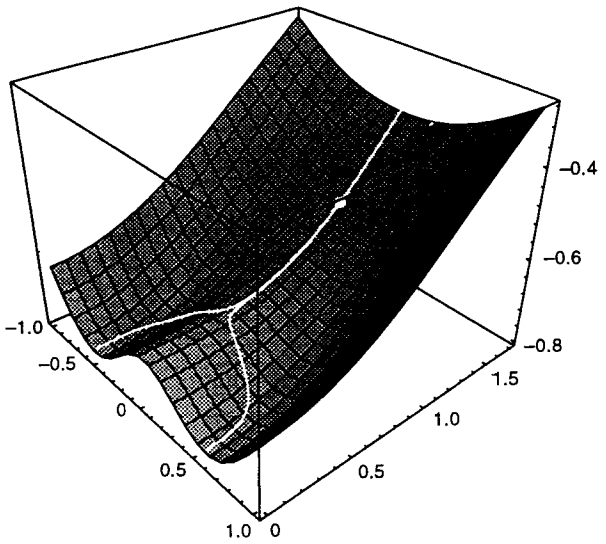

Fig. 1 Model potential-energy surface showing a bifurcating valley and a VRI. Two paths of steepest descent, displaced a small distance either side of the VRI follow the ridge for a considerable distance beyond the VRI before diverging.

potential-energy surfaces calculated by electronic structure methods.

Although Ruedenberg has clearly stated that the valley, not the reaction path, divides at the VRI, there may still be a general misconception that the reaction path also splits in two at the VRI. Ruedenberg has pointed out that the path does not bifurcate at a VRI unless it is a stationary point, and that for a non-stationary point, the path of steepest descent follows the ridge. Even when they are displaced a small amount to either side of the ridge, paths of steepest descent follow the ridge for a considerable distance before diverging (see Fig. 1). By way of comparison, note that paths infinitesimally displaced either side of the valley converge. The dilemma is then to develop a concept of a bifurcating reaction path that follows the valleys and not the ridge.

For a normal path of steepest descent, one can think of a marble rolling down the potential-energy surface very slowly (*e.g.* in molasses). We suggest for a bifurcating path, one should consider a pair of marbles, side by side, rolling slowly down the surface. The hard-sphere repulsion keeps them separated by a fixed distance and the paths are parallel to the path of steepest descent until the VRI is reached. After the VRI, the paths diverge, as shown in Fig. 2. The rate of divergence depends on the distance from the ridge, the slope along the path and the vibrational modes perpendicular to path. This concept can be generalized to many hard-sphere test particles descending on a surface. The resulting paths are similar to streamlines in incompressible fluid flow. For a wavepacket following the path, it is perhaps better considered as compressible fluid and to replace the hard-sphere potential with a softer repulsive potential [*e.g.* $1/r$, $1/r^2$, $\exp(-\alpha r^2)$]. One could even speculate that it may be possible to choose a form of this repulsion so that the streamlines correspond to lines of equal probability along a wavepacket trajectory.

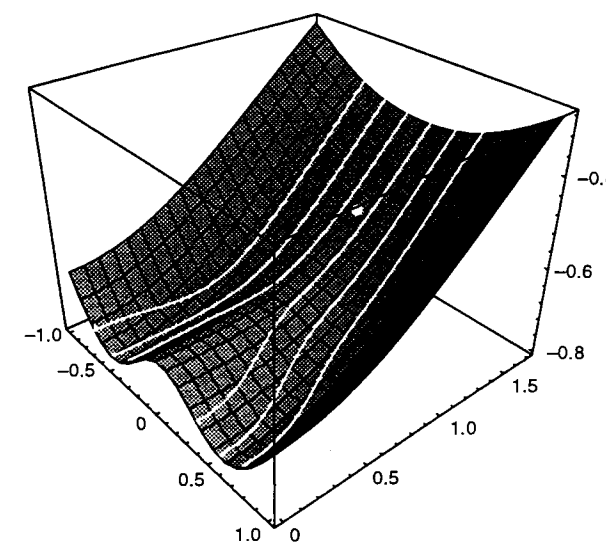

Fig. 2 A family of paths descending on a model potential-energy surface with a bifurcating valley and a VRI. A hard-sphere potential prevents the paths from coming closer than a preset minimum distance.

Relation between Errors in the Reaction Path, Tangent, Curvature and Projected Frequencies

A little work with a model potential can reveal some interesting connections between various errors encountered in reaction-path following. Consider a simple two-dimensional linear trough:

$$E(x, y) = -ax + \tfrac{1}{2}by^2; \quad \boldsymbol{g} = (-a, by); \quad \boldsymbol{H} = \begin{bmatrix} 0 & 0 \\ 0 & b \end{bmatrix} \tag{8}$$

Let the previous, current and next points on the reaction path be $\boldsymbol{x}_{-1} = (-c, 0)$, $\boldsymbol{x}_0 = (-0, 0)$ and $\boldsymbol{x}_1 = (c, 0)$; for each point the tangent and curvature are $\boldsymbol{v}^0 = (1, 0)$ and $\boldsymbol{v}^1 = (0, 0)$, respectively. Consider an error in the lateral position of the current point, $\boldsymbol{x}'_0 = (0, \Delta y)$. The tangent and curvature at this point can be found by substituting into eqn. (3) and (4):

$$\boldsymbol{v}'^0 = \frac{(a, -b\,\Delta y)}{\sqrt{(a^2 + b^2\,\Delta y^2)}} = (\cos\theta, -\sin\theta); \quad \tan\theta = b\,\Delta y/a \tag{9}$$

$$\boldsymbol{v}'^1 = -\frac{(0, -b\sin\theta) - b\sin^2\theta(\cos\theta, -\sin\theta)}{\sqrt{(a^2 + b^2\,\Delta y^2)}}$$

$$= \frac{b\cos\theta\sin\theta}{\sqrt{(a^2 + b^2\,\Delta y^2)}}(\sin\theta, \cos\theta) = \kappa(\sin\theta, \cos\theta) \tag{10}$$

For small displacements such that $a^2 \gg b^2\,\Delta y^2$, the tangent and the magnitude of the curvature are approximately

$$\boldsymbol{v}'^0 \approx (1, -b\,\Delta y/a); \quad \kappa \approx b^2\,\Delta y/a^2 \tag{11}$$

Thus the error in the tangent is a factor of b/a times the error in the coordinate of the reaction path. This factor can be significantly larger than 1 if a, the gradient along the path, is small (*e.g.* near the transition state) and/or if b, the second derivative perpendicular to the path, is large (*e.g.* a narrow valley). The amplification factor for the error in the curvature is the square of the factor for the tangent, indicating that it is even more difficult to compute accurate values for the curvature, and quantities that depend on it, such as the coupling coefficients in eqn. (7). The relative error in the projected frequency

$$\frac{\omega_0 - \omega}{\omega_0} = \frac{\sqrt{(b)} - \sqrt{(b\cos^2\theta)}}{\sqrt{(b)}} = 1 - \cos\theta \approx \frac{b^2\,\Delta y^2}{2a^2} \tag{12}$$

is smaller than the error in the tangent, since $b\,\Delta y/a < 1$. The errors in the normal modes are similar to the error in the tangent vector.

This analysis suggests that the coordinates of the reaction path need to be determined quite accurately near the transition state where the gradients are small, and for those in

perpendicular mode with large force constants. This also suggests some strategies for improving the calculations.

For first-order methods, one can obtain a suitable estimate of the tangent from the displacement

$$\boldsymbol{v}^0_{\text{est}} = \frac{\boldsymbol{x}'_0 - \boldsymbol{x}_{-1}}{|\boldsymbol{x}'_0 - \boldsymbol{x}_{-1}|} = \frac{(c, \Delta y)}{\sqrt{(c^2 + \Delta y^2)}} = (\cos\theta, -\sin\theta)$$

$$\tan\theta = -\Delta y/c \quad (13)$$

This will lead to an improvement in the curvature and projected frequencies if $1/c < b/a$. Note that the errors in $\boldsymbol{v}'^0$ and $(\boldsymbol{x}'_0 - \boldsymbol{x}_{-1})/|\boldsymbol{x}'_0 - \boldsymbol{x}_{-1}|$ are opposite in sign; if the two factors are comparable in magnitude, an improved estimate of the tangent is

$$\boldsymbol{v}^0_{\text{est}} = \left(\boldsymbol{v}'^0 + \frac{\boldsymbol{x}'_0 - \boldsymbol{x}_{-1}}{|\boldsymbol{x}_0 - \boldsymbol{x}_{-1}|}\right) \Big/ \left|\boldsymbol{v}'^0 + \frac{\boldsymbol{x}_0 - \boldsymbol{x}_{-1}}{|\boldsymbol{x}_0 - \boldsymbol{x}_{-1}|}\right| \quad (14)$$

If subsequent points along the path have already been calculated, a better estimate can be obtained by central difference:

$$\boldsymbol{v}^0_{\text{est}} = \frac{\boldsymbol{x}_1 - \boldsymbol{x}_{-1}}{|\boldsymbol{x}_1 - \boldsymbol{x}_{-1}|} \quad (15)$$

For higher-order explicit methods for reaction-path following, such as LQA and CLQA,[11] the estimated tangent analogous to eqn. (13) can be obtained by integrating the path and averaging the tangent of the integrated path and the calculated tangent, *e.g.*,

$$\boldsymbol{v}^0_{\text{LQA}} = \frac{-(\boldsymbol{g}_{-1} + \boldsymbol{H}_{-1}\Delta\boldsymbol{x}_{\text{LQA}})}{|\boldsymbol{g}_{-1} + \boldsymbol{H}_{-1}\Delta\boldsymbol{x}_{\text{LQA}}|};$$

$$\Delta\boldsymbol{x}_{\text{LQA}} = \int \frac{-\{\boldsymbol{g}_{-1} + \boldsymbol{H}_{-1}[\boldsymbol{x}(s) - \boldsymbol{x}_{-1}]\}}{|\boldsymbol{g}_{-1} + \boldsymbol{H}_{-1}[\boldsymbol{x}(s) - \boldsymbol{x}_{-1}]|}\,\mathrm{d}s \quad (16)$$

$$\boldsymbol{v}^0_{\text{est}} = (\boldsymbol{v}'^0 + \boldsymbol{v}^0_{\text{LQA}})/|\boldsymbol{v}'^0 + \boldsymbol{v}^0_{\text{LQA}}| \quad (17)$$

An improved estimate in the spirit of eqn. (15) can be obtained by matching the path integrated forward from the previous point and backward from the next point, and averaging the two tangents.

This approach can be taken one step further to calculate a local correction to the coordinates of the reaction path, based on the gradient and Hessian, and the estimated tangent from above. This can be done by minimizing in the space perpendicular to the estimated tangent:

$$\Delta\boldsymbol{x}_0 = -\boldsymbol{H}_0^{-1}[\boldsymbol{g}_0 - (\boldsymbol{g}_0^{\text{t}}\boldsymbol{v}^0_{\text{est}})\boldsymbol{v}^0_{\text{est}}] \quad (18)$$

$$\boldsymbol{v}^0 = -(\boldsymbol{g}_0 + \boldsymbol{H}_0\,\Delta\boldsymbol{x}_0)/|\boldsymbol{g}_0 + \boldsymbol{H}_0\,\Delta\boldsymbol{x}_0| \quad (19)$$

The new tangent and the current Hessian can then be used to calculate improved estimates of the curvature and projected frequencies. It should be emphasized that the effect of this correction is to clean up small errors in the path coordinates, and not to increase the order of the reaction-path following method. If eqn. (14), or its higher-order analogues such as eqn. (16), are used to estimate the tangent, this approach can be viewed as a generalization of the stabilization method used to improve the behaviour of the Euler method for reaction-path following.[12]

New Fourth-order Methods for Reaction-path Following

Numerical methods for integrating differential equations can be divided into two categories. For implicit methods, the step taken depends on the gradient at the end of the step, whereas for explicit methods it does not. Following reaction paths by the latter technique is computationally simpler and algorithms that have been used include Euler's method, the Ishida–Morokuma–Komornicki or stabilized Euler method (IMK or ES),[12] Runge–Kutta and predictor–corrector methods,[13] the local quadratic approximation (LQA),[11] LQA with cubic correction (CLQA),[11] and the Sun–Ruedenberg modification of LQA.[14] These methods employ a fixed number of calculations per step; some require only gradients and must take relatively small steps; others use second derivatives and have somewhat greater stability. Implicit methods are more difficult to implement, since the end-point of a step must be found by an optimization.[15,16] In return, these methods are more stable than explicit methods and can perform well with larger step sizes. Implicit methods for reaction path following include the Müller–Brown method (implicit Euler),[17] the second-order method of Gonzalez and Schlegel[15] (implicit trapezoid) and higher-order implicit methods by Gonzalez and Schlegel.[16]

For use with variational transition-state theory and reaction-path Hamiltonian calculations, it is highly desirable to combine the stability of implicit methods yet avoid the constrained optimization used to determine the end-point of a step. The method should also be higher than second order (so that larger steps can be taken) and use the gradient and Hessian at each point on the path (since the rate calculations need the Hessian at each point). We have combined ideas from the local corrections discussed above and from various implicit and explicit methods to devised two new fourth-order reaction-path following algorithms.

Method 1 combines an LQA predictor step[11] with a corrector step based on the fourth-order method F of Gonzalez and Schlegel.[16] The LQA step is obtained by integrating a local quadratic approximation for the gradient from $\boldsymbol{x}_1$, the current point on the path to $\boldsymbol{x}'_2$:

$$\frac{\mathrm{d}\boldsymbol{x}(s)}{\mathrm{d}s} = \frac{-\boldsymbol{g}'_1 + \boldsymbol{H}'_1(\boldsymbol{x} - \boldsymbol{x}'_1)}{|\boldsymbol{g}'_1 + \boldsymbol{H}'_1(\boldsymbol{x} - \boldsymbol{x}'_1)|} \quad (20)$$

where $\boldsymbol{g}'_1$ and $\boldsymbol{H}'_1$ are the gradient and Hessian calculated at $\boldsymbol{x}'_1$, a point near $\boldsymbol{x}_1$. The gradient and Hessian, $\boldsymbol{g}'_2$ and $\boldsymbol{H}'_2$, are then calculated at $\boldsymbol{x}'_2$. Eqn. (3) and (4) are used to calculate $\boldsymbol{v}^0(0)$ and $\boldsymbol{v}^1(0)$ from $\boldsymbol{g}_1 \approx \boldsymbol{g}'_1 + \boldsymbol{H}'_1(\boldsymbol{x}_1 - \boldsymbol{x}'_1)$ and $\boldsymbol{H}_1 \approx \boldsymbol{H}'_1$; likewise $\boldsymbol{v}^0(s)$ and $\boldsymbol{v}^1(s)$ are calculated from $\boldsymbol{g}_2 \approx \boldsymbol{g}'_2 + \boldsymbol{H}'_2(\boldsymbol{x}_2 - \boldsymbol{x}'_2)$ and $\boldsymbol{H}_2 \approx \boldsymbol{H}'_2$. Then $\boldsymbol{x}_2$ is adjusted iteratively until eqn. (21) (the defining equation for method F[16]) is satisfied,

$$\boldsymbol{x}_2 = \boldsymbol{x}_1 + \tfrac{1}{2}[\boldsymbol{v}^0(0) + \boldsymbol{v}^0(s)]s + \tfrac{1}{2}[\boldsymbol{v}^1(0) - \boldsymbol{v}^1(s)]s^2 \quad (21)$$

where s is chosen to minimize $|\boldsymbol{x}_2 - \boldsymbol{x}'_2|$. Because method F is correct to fourth order, the resulting step from $\boldsymbol{x}_1$ to $\boldsymbol{x}_2$ is also fourth order, provided that $|\boldsymbol{x}_1 - \boldsymbol{x}'_1|$ and $|\boldsymbol{x}_2 - \boldsymbol{x}'_2|$ are sufficiently small so that local quadratic approximations around $\boldsymbol{x}'_1$ and $\boldsymbol{x}'_2$ are valid.

Method 2 combines an LQA step with an integration on a quartic surface. The LQA step from $\boldsymbol{x}_1$ to $\boldsymbol{x}'_2$ and the calculation of $\boldsymbol{g}'_2$ and $\boldsymbol{H}'_2$ are the same as in method 1. A quartic energy surface (cubic surface for the gradient) is constructed by fitting to the gradients $\boldsymbol{g}'_1$, $\boldsymbol{g}'_2$ and the Hessians $\boldsymbol{H}'_1$ and $\boldsymbol{H}'_2$.

$$\begin{aligned}\boldsymbol{g}(x) = {} & \{\boldsymbol{g}'_1 + \boldsymbol{H}'_1[(\boldsymbol{x} - \boldsymbol{x}'_1) - t(\boldsymbol{x}'_2 - \boldsymbol{x}'_1)]\}f_1(t) \\ & + \boldsymbol{H}'_1(\boldsymbol{x}'_2 - \boldsymbol{x}'_1)f_2(t) \\ & + \{\boldsymbol{g}'_2 + \boldsymbol{H}'_2[(\boldsymbol{x} - \boldsymbol{x}'_2) - (1 - t)(\boldsymbol{x}'_2 - \boldsymbol{x}'_1)]\} \\ & \times f_1(1 - t) + \boldsymbol{H}'_2(\boldsymbol{x}'_1 - \boldsymbol{x}'_2)f_2(1 - t) \quad (22)\end{aligned}$$

$$t = (\boldsymbol{x} - \boldsymbol{x}'_1)(\boldsymbol{x}'_2 - \boldsymbol{x}'_1)/|\boldsymbol{x}'_2 - \boldsymbol{x}'_1|^2$$

$$f_1(t) = 1 - 3t^2 + 2t^3; \quad f_2(t) = t - 2t^2 + t^3$$

This approximation for the gradient is used in eqn. (3) and the reaction path between $\boldsymbol{x}_1$ and $\boldsymbol{x}_2$ is obtained by integrating the differential equation using an accurate numerical method such as the Bulirsch–Stoer method.[18]

Both methods outlined above are fourth order, but they have different contributions from higher-order terms. Since they use the same information (g'_1, g'_2, H'_1, H'_2), one can readily compute the step along the path by both methods. The difference between the two paths gives an estimate of the error in the reaction-path following. If this error estimate is outside the acceptable range, the size of the next step can be adjusted accordingly. If the corrections to the LQA step become sizeable, it may be better to calculate x'_2 by the CLQA method,[11] or by integrating the quartic approximation from the previous step.

Test Surfaces for Reaction-path Following

Four surfaces are considered in this section: the quadratic and helical valleys are special because they are treated exactly by the LQA and second-order Gonzalez–Schlegel methods, respectively; the Fresnel and logarithmic spirals are important because they have a very simple dependence on the curvature on the reaction path.

A quadratic surface for testing reaction-path following is almost trivial, but is of some interest because the path can be obtained analytically, and because the LQA algorithm (and any method derived from it) is exact for this class of surfaces. For simplicity, consider a two-dimensional surface where the eigenvectors of the Hessian aligned with the axes and the minimum is at the origin; the surface, path of steepest descent, tangent and curvature are:

$$E = \tfrac{1}{2}ax^2 + \tfrac{1}{2}by^2; \quad \boldsymbol{g} = (ax, by) \tag{23}$$

$$\boldsymbol{x}(s) = [x_0 \exp(-at), y_0 \exp(-bt)];$$

$$\frac{ds}{dt} = \sqrt{[a^2x_0^2 \exp(-2at) + b^2y_0^2 \exp(-2bt)]} \tag{24}$$

$$\boldsymbol{v}^0 = \frac{[-ax_0 \exp(-at), -by_0 \exp(-bt)]}{\sqrt{[a^2x_0^2 \exp(-2at) + b^2y_0^2 \exp(-2bt)]}}$$

$$= (\cos\theta, \sin\theta) \tag{25}$$

$$\tan\theta = \frac{by_0}{ax_0}\exp[-(b-a)t]; \quad \frac{d\theta}{dt} = -\frac{b-a}{2}\sin 2\theta$$

$$\boldsymbol{v}^1 = \frac{d\boldsymbol{v}^0}{ds} = \frac{d\boldsymbol{v}^0}{d\theta}\frac{d\theta}{dt}\frac{dt}{ds} = \kappa(\sin\theta, -\cos\theta) \tag{26}$$

$$\kappa = \left|\frac{d\theta}{dt}\frac{dt}{ss}\right| = \frac{(b-a)\sin 2\theta}{2\sqrt{[a^2x_0^2 \exp(-2at) + b^2y_0^2 \exp(-2bt)]}}$$

Fig. 3 shows a typical path. For equal displacements along both axes, the descent is first along the mode with the largest eigenvalue until the gradient for this mode becomes comparable to the gradient along the other modes. Thus, many of the regions of high curvature seen in reaction paths arise when the descent along one mode is nearly complete and the path turns to descend along another mode. The magnitude of the curvature, κ, reaches a maximum near $\theta = \pi/4$, and the value at the maximum depends primarily on the difference in the eigenvalues.

A series of incrementally more challenging test functions can be constructed to have analytical reaction paths with the following properties: (*a*) zero curvature [$\kappa = 0$, a linear trough, eqn. (8)], (*b*) constant curvature (κ = constant, circular helix), (*c*) curvature linearly dependent on the arc length ($\kappa = \alpha s$, a Fresnel spiral) and (*d*) curvature inversely dependent on the arc length ($\kappa = \alpha/s$, a logarithmic spiral).

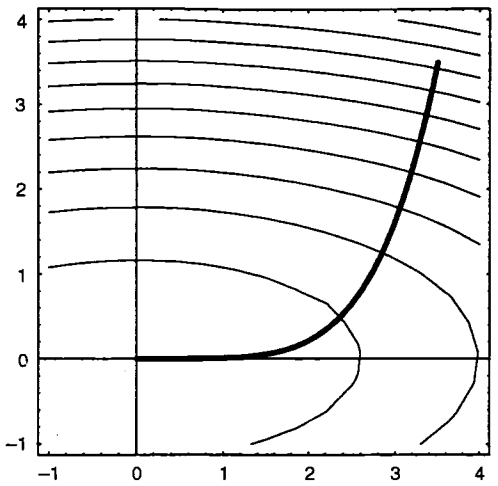

Fig. 3 A simple quadratic surface showing a path of steepest descent. The maximum curvature depends on the difference in the eigenvalues.

A circular helix, shown in Fig. 4, is a three-dimensional curve with constant curvature, κ, and torsion, τ. We have devised a simple potential whose reaction path is a circular helix:

$$E(r, \theta, z) = bz + \frac{c}{2}(r - r_0)^2 + \frac{d}{2}\left[1 - \cos\left(\frac{z}{a} - \theta + \theta_0\right)\right];$$

$$\sin\theta_0 = -\frac{-2ab}{(1+a^2)d} \tag{27}$$

$$\boldsymbol{x}(s) = (r_0\cos\theta, r_0\sin\theta, a\theta); \quad s = \theta\sqrt{(r_0^2 + a^2)} \tag{28}$$

$$\boldsymbol{v}^0(s) = (-r_0\sin\theta, r_0\cos\theta, a)/\sqrt{(r_0^2 + a^2)} \tag{29}$$

$$\boldsymbol{v}^1(s) = (-r_0\cos\theta, -r_0\sin\theta, 0)/(r_0^2 + a^2);$$

$$\kappa = r_0/(r_0^2 + a^2) \tag{30}$$

The second-order and fourth-order method F of Gonzalez and Schlegel are exact for this class of surfaces if they are started on the path, but methods such as LQA, CLQA and

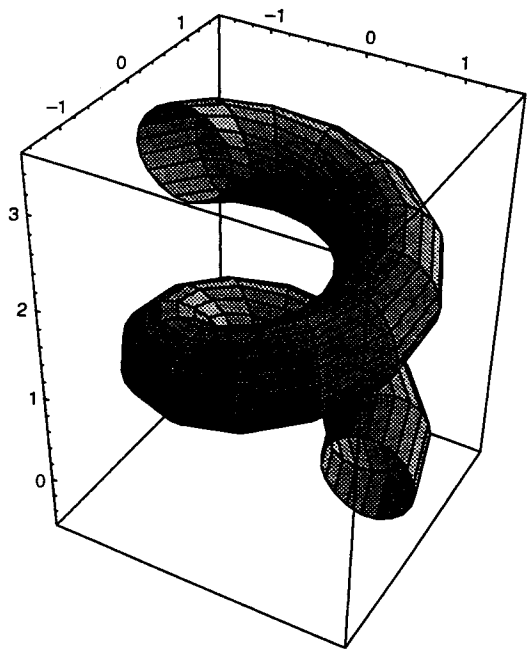

Fig. 4 Three-dimensional contour for the helical valley, eqn. (27) with $a = 1/\pi$, $b = 0$ and $c = 4d$

traditional numerical methods for integrating differential equations are not.

Integration of the appropriate equations for $\kappa = \pi s$ leads to the Fresnel integrals[19]

$$x(s) = [C(s), S(s)]; \quad C(s) = \int_0^s \cos \pi x^2/2 \, dx;$$

$$S(s) = \int_0^s \sin \pi x^2/2 \, dx \tag{31}$$

$$v^0(s) = (\cos \theta, \sin \theta); \quad \theta = \pi s^2/2 \tag{32}$$

$$v^1(s) = \kappa(-\sin \theta, \cos \theta); \quad \kappa = \pi s \tag{33}$$

The reaction path, a Fresnel spiral, is shown in Fig. 5 and for large s has the limiting behaviour of $r^2\theta = \text{const}$. Despite the simple functional form of κ, none of the reaction-path algorithms devised so far (including method F) is exact for the Fresnel spiral.

A logarithmic spiral is obtained if one integrates the equations of $\kappa = a/s$, where s is the distance from the centre of the spiral. We have constructed a simple energy surface with a logarithmic spiral as a reaction path.

$$E(r, \theta) = \frac{b}{2}\left[1 - \cos\left(\frac{\ln r}{a} - \theta + \theta_0\right)\right] + c \ln r$$

$$= \frac{b}{2}\left[1 - \frac{x}{r}\cos\left(\frac{\ln r}{a} + \theta_0\right) - \frac{y}{r}\cos\left(\frac{\ln r}{a} + \theta_0\right)\right] + c \ln r \tag{34}$$

$$\sin \theta_0 = -2ac/(1 + a^2)b$$

$$x(s) = \exp(a\theta)(\cos \theta, \sin \theta); \quad s = \sqrt{(1 + a^2)}\exp(a\theta)/a \tag{35}$$

$$v^0(s) = (a \cos \theta - \sin \theta, a \sin \theta + \cos \theta)/\sqrt{(1 + a^2)} \tag{36}$$

$$v^1(s) = \frac{-a \sin \theta - \cos \theta, a \cos \theta - \sin \theta}{[(1 + a^2)\exp(a\theta)]}; \quad \kappa = a/s \tag{37}$$

The surface is shown in Fig. 6. Like the Fresnel spiral, none of the reaction-path methods developed to date are exact for the logarithmic spiral.

Fig. 6 shows a contour plot of the surface and compares reaction-path following methods 1 and 2 of the present work with the LQA method of Page and McIver, the second-order methods Gonzalez–Schlegel and the exact path. When the valley is broad and the curvature small compared to the step size, then all methods behave quite well. As the valley becomes narrower and more curved, methods 1 and 2 perform better than LQA. All of the methods eventually fail when the valley becomes too high and curved for a given step size.

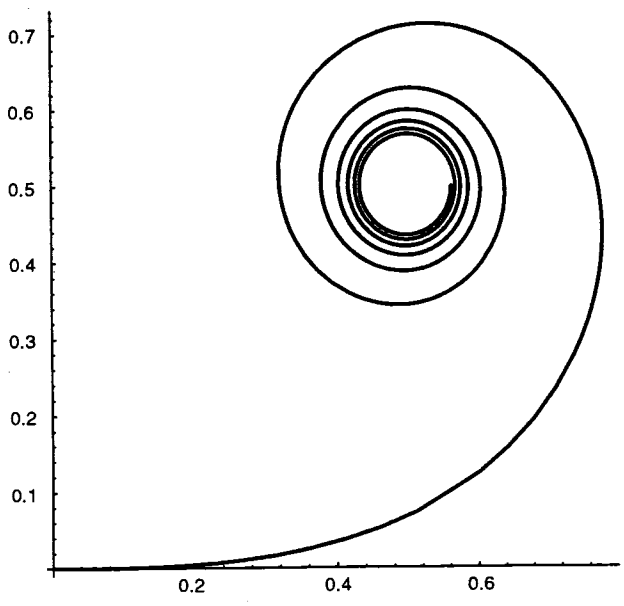

Fig. 5 A Fresnel spiral, $x = [C(s), S(s)]$ [see eqn. (31)–(33)]

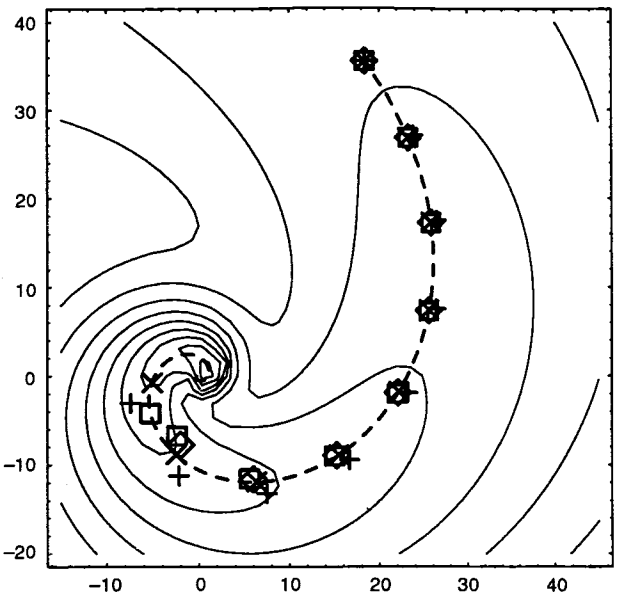

Fig. 6 Contour plot of a logarithmic spiral valley [eqn. (34), $a = \frac{1}{2}$, $b = 1$, $c = \frac{1}{2}$] and a comparison of reaction-path following methods 1 (◇) and 2 (□) with LQA (+), second-order GS (×) and the exact path (– – –)

Summary

A number of thoughts on reaction-path following have been collected together in this paper. To address the dilemma of bifurcation, we offer the concept of a set of hard-sphere test particles descending the surface, tracing out paths akin to streamlines, that follow the bifurcating valleys. We have used a simple model to analyse errors in reaction-path following and have proposed a local correction method that is a generalization of the Euler stabilization approach. We have developed two new fourth-order reaction-path following methods that make maximal use of the gradient and Hessian at each step. Lastly, we have examined a number of test surfaces and devised two new potentals with analytical reaction paths.

References

1 J. B. Foresman and A. Frisch, *Exploring Chemistry with Electronic Structure Methods*, Gaussian Inc., 1993.
2 K. Fukui, *Acc. Chem. Res.*, 1981, **14**, 363.
3 J. I. Steinfeld, J. S. Francisco and W. L. Hase, *Chemical Kinetics and Dynamics*, Prentice-Hall, New Jersey, 1989.
4 D. G. Truhlar and M. S. Gordon, *Science*, 1990, **249**, 491.
5 M. L. McKee and M. Page, *Rev. Comput. Chem.*, 1993, **4**, 35.
6 H. B. Schlegel, in *Modern Electronic Structure Theory*, ed. D. R. Yarkony, World Scientific Publishing, Singapore, in the press.
7 D. G. Truhlar and B. C. Garrett, *Acc. Chem. Res.*, 1980, **13**, 440.
8 W. H. Miller, N. C. Handy and J. E. Adams, *J. Chem. Phys.*, 1980, **72**, 99.
9 P. Valtazanos and K. Ruedenberg, *Theor. Chim. Acta*, 1986, **69**, 281.
10 J. Baker and P. M. W. Gill, *J. Comput. Chem.*, 1988, **9**, 465.

11 M. Page and J. M. McIver, *J. Chem. Phys.*, 1988, **88**, 922; M. Page, C. Doubleday and J. W. McIver, *J. Chem. Phys.*, 1990, **93**, 5634.
12 K. Ishida, K. Morokuma and A. Komornicki, *J. Chem. Phys.*, 1977, **66**, 2153; M. W. Schmidt, M. S. Gordon and M. Dupuis, *J. Am. Chem. Soc.*, 1985, **107**, 2585.
13 B. C. Garrett, M. J. Redmon, R. Steckler, D. G. Truhlar, K. K. Baldridge, D. Bartol, M. W. Schmidt and M. S. Gordon, *J. Phys. Chem.*, 1988, **92**, 1476; K. K. Baldridge, M. S. Gordon, R. Steckler and D. G. Truhlar, *J. Phys. Chem.*, 1989, **93**, 5107.
14 J. Q. Sun and K. Ruedenberg, *J. Chem. Phys.*, 1993, **99**, 5257.
15 C. Gonzalez and H. B. Schlegel, *J. Chem. Phys.*, 1989, **90**, 2154; C. Gonzalez and H. B. Schlegel, *J. Phys. Chem.*, 1990, **94**, 5523.
16 C. Gonzalez and H. B. Schlegel, *J. Chem. Phys.*, 1991, **95**, 5853.
17 K. Müller and L. D. Brown, *Theor. Chim. Acta*, 1979, **53**, 75.
18 W. H. Press, B. P. Flannery, S. A. Teukolsky and W. T. Vetterling, *Numerical Recipes*, Cambridge University Press, Cambridge, 1989.
19 M. Abramowitz and I. A. Stegan, *Handbook of Mathematical Functions*, Dover Press, New York, 1965.
20 S. Wolfram, *Mathematica*, Addison Wesley, London, 1988, and associated computer programs were used to carry out the calculations and prepare the plots in this paper.

Paper 3/05186B; *Received 27th August*, 1993